JJEE
Volume 1, Number 1, 2015
Pages 13-24
Jordan Journal of Electrical Engineering
ISSN (Print): 2409-9600, ISSN (Online): 2409-9619

Analysis of Brushless DC Motor with Trapezoidal Back EMF using MATLAB

Taha A. Hussein

Foundation of Technical Education, Technical College, Mosul, Iraq
e-mail: taha_hussian@yahoo.com

Received: January 14, 2015 *Accepted: March 7, 2015*

***Abstract*—** The dynamic characteristics such as speed and torque as well as voltages and currents of PWM brushless DC motor inverter are analyzed with a MATLAB model. The contribution of external load torque and friction torque is monitored. The switching function technique is adopted for the current control of the embedded three-phase inverter that drives the brushless DC motor. In switching functions, power conversion circuits can be modeled according to their functions rather than circuit topologies. Therefore, it can simplify the overall power conversion functions. The trapezoidal type (back EMF) is used in the model as it has lower switching loss compared with sinusoidal type (back EMF). Results show reliable time analysis of speed, torque, phase and line voltages and currents. The effect of current commutation is clearly observed.

***Keywords*—** Brushless DC motor, DC motor control, PWM inverter, ripple torque, trapezoidal back EMF.

I. INTRODUCTION

A three-phase brushless DC motor (BLDCM) consists of permanent magnet and excitation windings. Fig. 1 shows a particular type of twelve-pole/nine-slot BLDCM. A three-phase inverter is used to supply the stator as shown in Fig. 2. The stator and rotor fields are designed to be perpendicular in order to create maximum torque. This feature is achieved by proper commutation of inverter, which acts as a commutator and brush of conventional DC motors [1]. BLDCM has high dynamic response compared with brushed DC motors. Also it has better speed versus torque characteristics, noiseless operation and high operating ranges. BLDCM is widely used in most industrial automation equipment such as robotics, medical, aerospace and so on. Simulation models of BLDCM are based in most cases on state space equations, Fourier analysis, and the *d-q* axis [2]. BLDCM can be classified as of sinusoidal or trapezoidal type according to the rotational voltage (back EMF) induced. Trapezoidal excitation has lower switching loss, while sinusoidal excitation has lower copper loss. The relatively low switching loss for trapezoidal excitation is due to the fact that only one phase is chopping at a frequency at a time, while in sinusoidal type all the three phases are chopping at the same time. In trapezoidal commutation, there will be higher torque ripple and a poor harmonic performance compared with almost no torque ripple and better harmonic performance in sinusoidal commutation [3]. This comparison means that trapezoidal commutation has advantage over sinusoidal commutation.

II. MODELING AND SIMULATION OF BLDCM DRIVE SYSTEM

Fig. 3 shows an equivalent circuit diagram for the BLDCM. The PWM inverter topology is a six-switch voltage source with DC-link (VD). Each phase of the three phases in BLDCM consists of a resistance, inductance, mutual inductance and back EMF [4].

Corresponding authors' e-mail: taha_hussian@yahoo.com

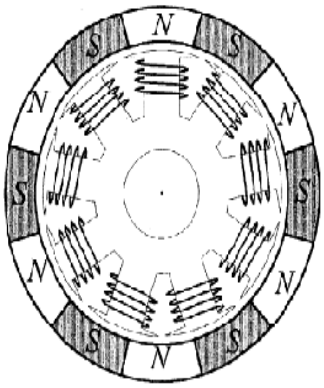

Fig. 1. Twelve-pole BLDCM

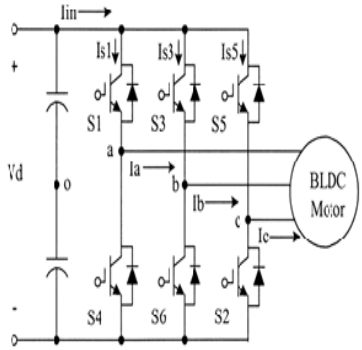

Fig. 2. Three-phase inverter

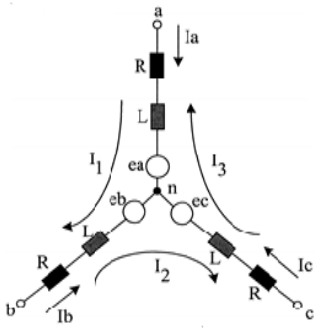

Fig. 3. Equivalent circuit diagram for the BLDCM

The dynamic equations of BLDCM are derived as follows:

$$V_{ab} = R_{LL} i_1 + (L - M)_{LL} \frac{di_1}{dt} + e_{ab} \quad (1)$$

$$V_{bc} = R_{LL} i_2 + (L - M)_{LL} \frac{di_2}{dt} + e_{bc} \quad (2)$$

$$V_{ca} = R_{LL} i_3 + (L - M)_{LL} \frac{di_3}{dt} + e_{ca} \quad (3)$$

where V_{ab}, V_{bc} and V_{ca} are line voltages, R_{LL} is the line-to-line resistance and equals $2R$, $(L - M)_{LL}$ is the line-to-line inductance and equals to $2(L - M)$, M is mutual inductance, e_{ab}, e_{bc} and e_{ca} are the line-to-line trapezoidal back EMF's. The electromagnetic torque equation is expressed as:

$$T_e = T_L + J \frac{dw_r}{dt} + B w_r \quad (4)$$

where T_e is the electromagnetic torque, T_L is the load torque, J is the inertia, B is the friction coefficient and w_r is the speed of BLDCM in electrical rad/s, where the relation between the electrical and mechanical rotor speed will be defined:

$$\frac{dw_r}{dt} = \frac{1}{J} (T_e - T_L - B w_r) \quad (5)$$

$$w_r = \frac{1}{J} \int (T_e - T_L - B w_r) dt \text{ and } \frac{d\theta}{dt} = w_r \rightarrow \theta_r = \int w_r \, dt \quad (6)$$

where θ_r is the position of the rotor. The mechanical rotor speed w_m in rad/s is calculated as:

$$w_m = \frac{2}{P} w_r \quad (7)$$

where P is the number of poles. In this work, the damping factor B is not neglected, as often in most papers, in order to find its contribution to the transient period. The three-phase currents are controlled in a type of quasi-square waveform in order to be synchronized with the trapezoidal back EMF to achieve the desired constant torque.

III. OVERALL SIMULINK BLOCK DIAGRAM FOR BLDCM

Fig. 4 shows the overall block diagram of the BLDCM drive. The main blocks are: back EMF, inverter block, current control block, and speed/torque block. Many important changes in the overall model are adopted in this paper compared with other works [5]-[9]. Among these changes are an addition of the effect of the friction torque and a reliable switching function model.

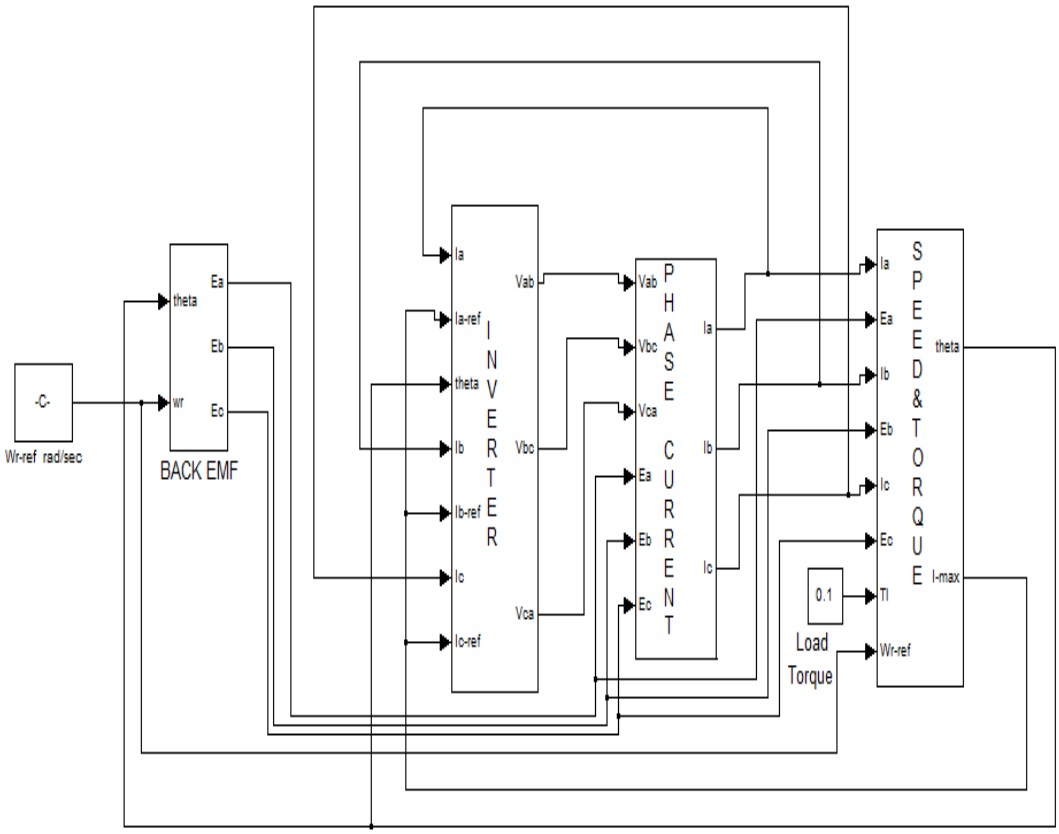

Fig. 4. Overall circuit diagram for BLDCM

A. Modeling of Trapezoidal Back EMF

The back EMF is a function of rotor position θ_r and has amplitude of:

$$E = k_e.w_r$$

where k_e is the back EMF constant. The three-phase back EMFs can be generated uniquely for every operating speed based on the rotor position θ_r as shown in Fig. 5. The numerical expression of the back EMF can be obtained as shown in Table 1. The back EMF is implemented with a series of IF blocks together with merge block to simulate the process in Table 1 as shown in Fig. 6 for phase *a*.

B. Speed and Torque Control Block

The electromagnetic torque is composed of ($T_e = T_a + T_b + T_c$) where T_a , T_b and T_c are the torques developed by phases *a*, *b* and *c* respectively. The load torque is subtracted from the electromagnetic torque to get the net torque, which drives the BLDCM. The torque and

speed control circuit can be implemented according to (4)-(7) as shown in Fig. 7. The output node 2 in Fig. 7 refers to reference current *I-max*, which is compared with actual load current to produce the switching functions. The function of the PI controller is to tune *I-max* to the optimum value that matches the transient period. The friction (*B* damping effect) is inserted as negative feedback coefficient at the inputs of torque box.

TABLE 1
GENERATION OF BACK EMF BASED ON ROTOR POSITION

θ_r (rotor position)	e_a (back EMF)	e_b (back EMF)	e_c (back EMF)
$0 < \theta_r < \pi/6$	$(6/\pi).\theta_r$	-1	1
$\pi/6 < \theta_r < \pi/2$	1	-1	$-(6/\pi).\theta_r + 2$
$\pi/2 < \theta_r < 5\pi/6$	1	$(6/\pi).\theta_r - 4$	-1
$5\pi/6 < \theta_r < 7\pi/6$	$-(6/\pi).\theta_r + 6$	1	-1
$7\pi/6 < \theta_r < 9\pi/6$	-1	1	$(6/\pi).\theta_r - 8$
$9\pi/6 < \theta_r < 11\pi/6$	-1	$-(6/\pi).\theta_r + 10$	1
$11\pi/6 < \theta_r < 2\pi$	$(6/\pi).\theta_r - 12$	-1	1

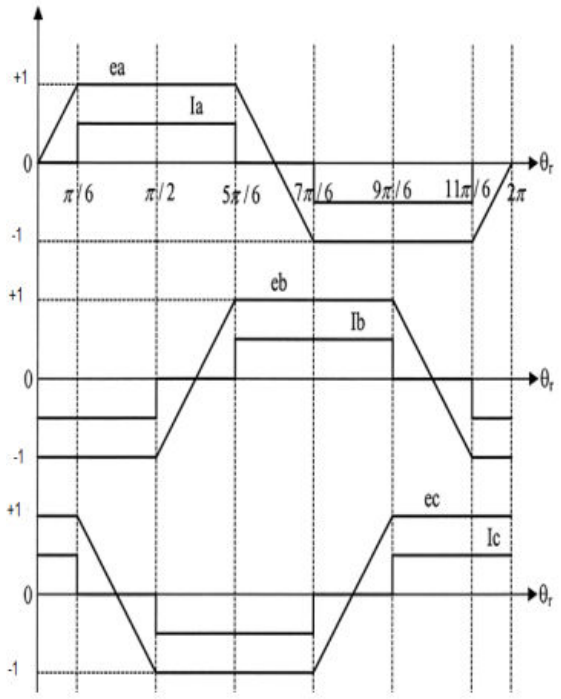

Fig. 5. Generation of back EMF

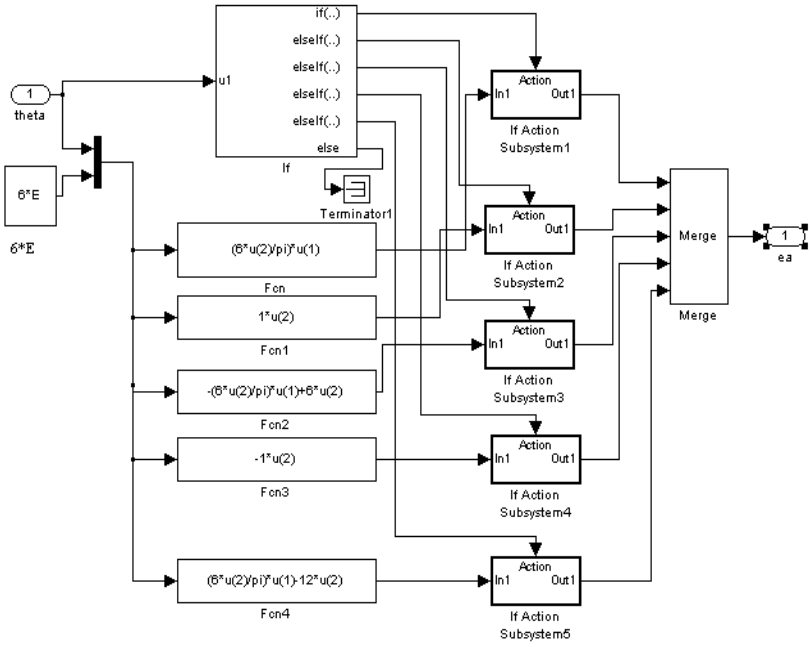

Fig. 6. Implementation of back EMF phase *a*

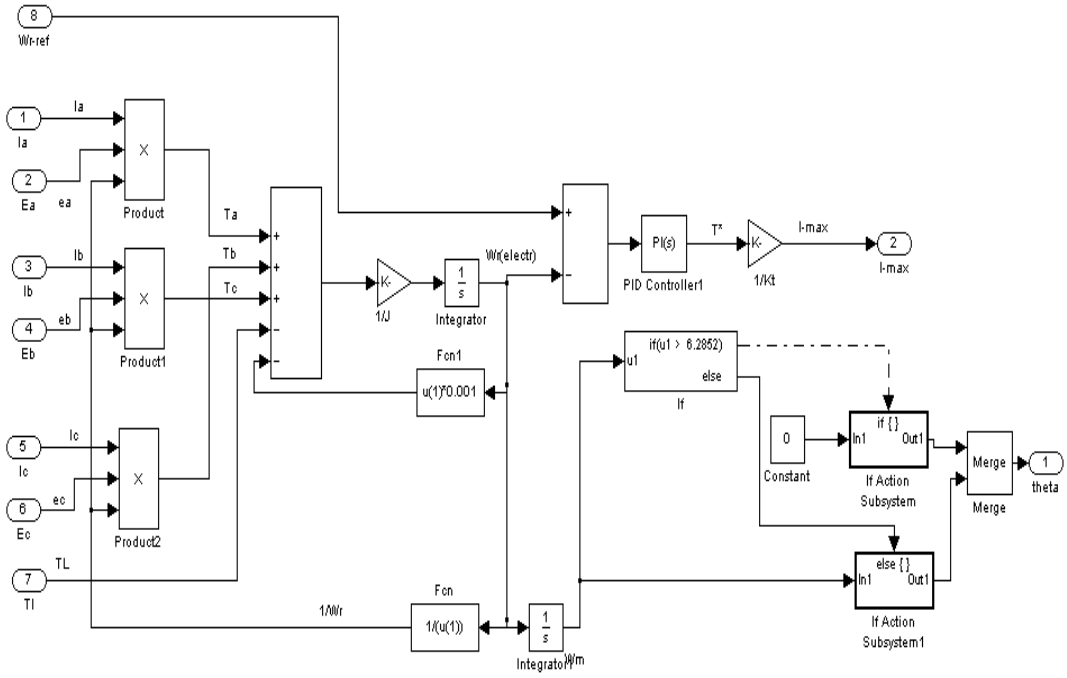

Fig. 7. Implementation of speed and torque including friction torque

C. Dynamic Response during Transient Analysis

The current control for phases *a*, *b*, and *c* can be divided into different periods following the polarity of the current. A reference current is needed to find the exact period of the actual current. An upper limit (UL) of (1.05 of the reference current) and a lower limit (LL) of (0.95 of the reference current) are used to find out which switch must be on or off in the inverter model. The actual current (load current) may have increasing or decreasing slops associated

with upper and lower limits as shown in Fig. 8. A memory block, which stores the previous value of its input, is used to simulate this differentiation process (i.e. $I_a^{'}$). Table 2 shows possible switch states results from the comparison between the load current and the reference current. These switching actions are used to control the inverter model.

TABLE 2
SWITCH STATES DEFINED BY LOWER AND UPPER LIMITS OF I-MAX COMPARED WITH LOAD CURRENT

$Ia > 0$	$Ia < LL$	$I_a > UL$	$LL < I_a < UL \;\&I_a^{'} > 0$	$LL < I_a < UL \;\&I_a^{'} < 0$
	$S_1\ on$	$S_1\ off\ D_4\ on$	$S_1\ 0n$	$S_1\ off\ D_4\ on$
$Ia < 0$	$I_a > UL$	$Ia <\ LL$	$LL < I_a < UL \;\&I_a^{'} < 0$	$LL < I_a < UL \;\&I_a^{'} > 0$
	$S_4\ 0n$	$S_4\ off\ D_1\ on$	S_4	$S_4\ off\ D_1\ on$

D. Switching Functions

Following Table 2, the switching function *SFa* is derived to control the current in phase *a* in the PWM inverter system. Other switching functions *SFb* and *SFc* are determined via comparing phase currents *Ib* and *Ic* with their respective reference currents. In switching functions, the power conversions circuits can be modeled according to their functions rather than circuit topologies [4]. Therefore, it simplify the overall power conversion functions. The detailed switching function of phase *a* is shown in Fig. 9.

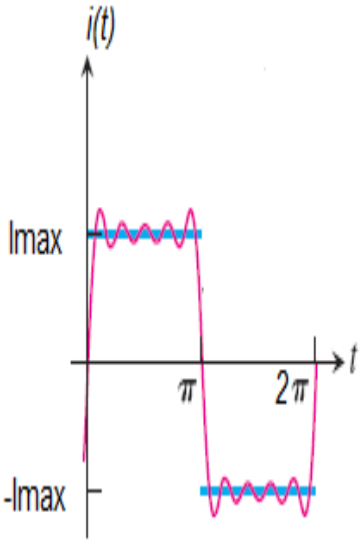

Fig. 8. Reference and load current

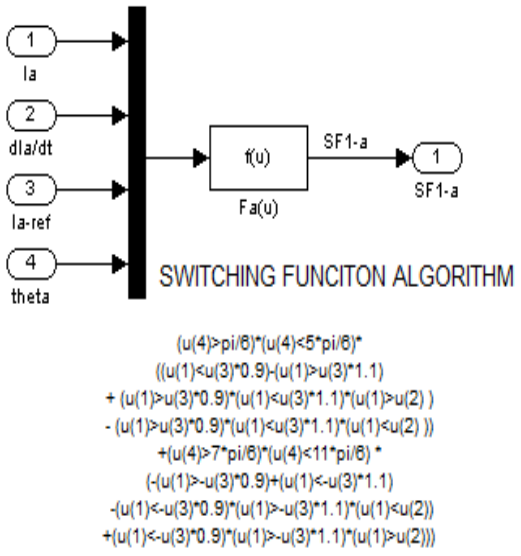

Fig. 9. Implementation of the switching function of phase *a*

E. Simulink Block for the Three-Phase Inverter Drive

From (1)-(3) together with switching functions the model for the inverter drive is shown in Fig. 10. Phase currents can be determined from line currents as follows:

$$i_a = i_1 - i_3\ ,\ \ i_b = i_2 - i_1,\ i_c = i_3 - i_2 \tag{8}$$

Then, the inverter line-to-line voltage can be derived as:

$$v_{ab} = v_{a0} - v_{b0} = \frac{v_d}{2}(SF_a - SF_b) \quad (9)$$

$$v_{bc} = v_{b0} - v_{c0} = \frac{v_d}{2}(SF_b - SF_c) \quad (10)$$

$$v_{ca} = v_{c0} - v_{a0} = \frac{v_d}{2}(SF_c - SF_a) \quad (11)$$

All values of currents and voltages, (i.e. rms, average etc.) can be calculated and manipulated easily in MATLAB workspace.

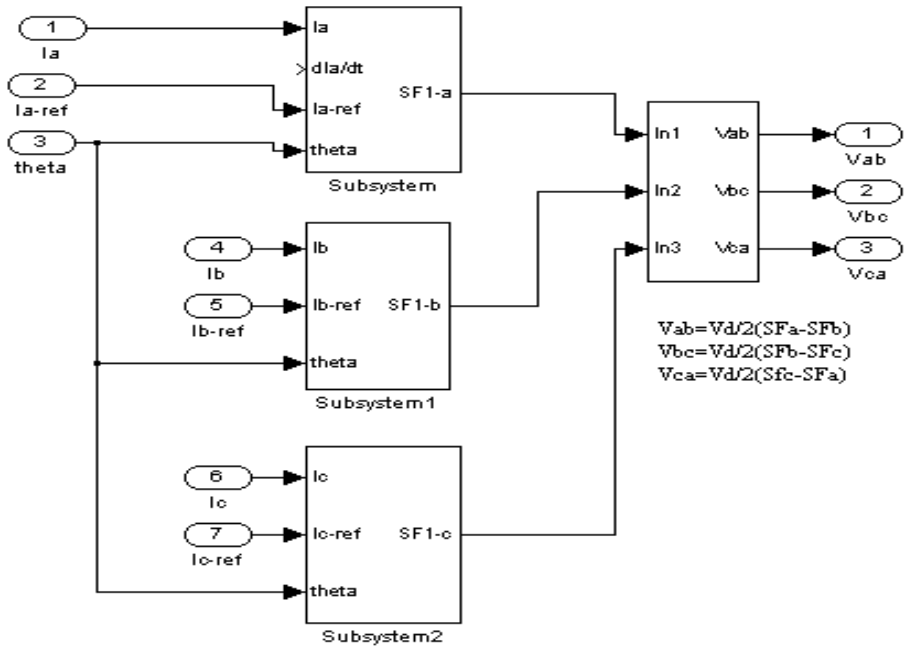

Fig. 10. Implementation of the three-phase inverter drive

IV. SIMULATION RESULTS

The specifications of the adopted BLDCM used for MATLAB simulation include: K_t=0.21476 Nm where K_t is the integration constant in (6), $K_{e\text{-}LL}$=0.21486 V/(rad/s) where $K_{e\text{-}LL}$ is the line to line back EMF constant, J=8.2614e^{-5} kg.m^2, T_L=0.662 Nm, R_{LL}=1.5Ω, $(L\text{-}M)_{LL}$=6.1mH, and rated mechanical speed ω_m=2500 rpm [5]. The three-phase symmetrical back EMF waveforms are generated according to Table 1 for phase and line voltages. Fig. 11-*a* shows back EMF's for phases *a*, *b* and *c* with reference to rotor position, which is varied from 0 to 2π per electric cycle. The corresponding back EMFs for line voltages are shown in Fig. 11-*b*. For 2500 rpm, the electric cycle is calculated as: $\omega_e = \omega_m(P/2)$, where ω_e is the electrical speed and P=2 is the number of pairs of poles. A simple calculation determines ω_e=41.66 cycles/s. The period of one cycle is T=1/41.66=0.024 s.

Fig. 12-*a* shows the phase currents I_a, I_b and I_c. The commutation takes place every 120° conduction period. This pulsating ripple is shown in Fig. 12-*b* for the line currents I_1, I_2 and I_3.

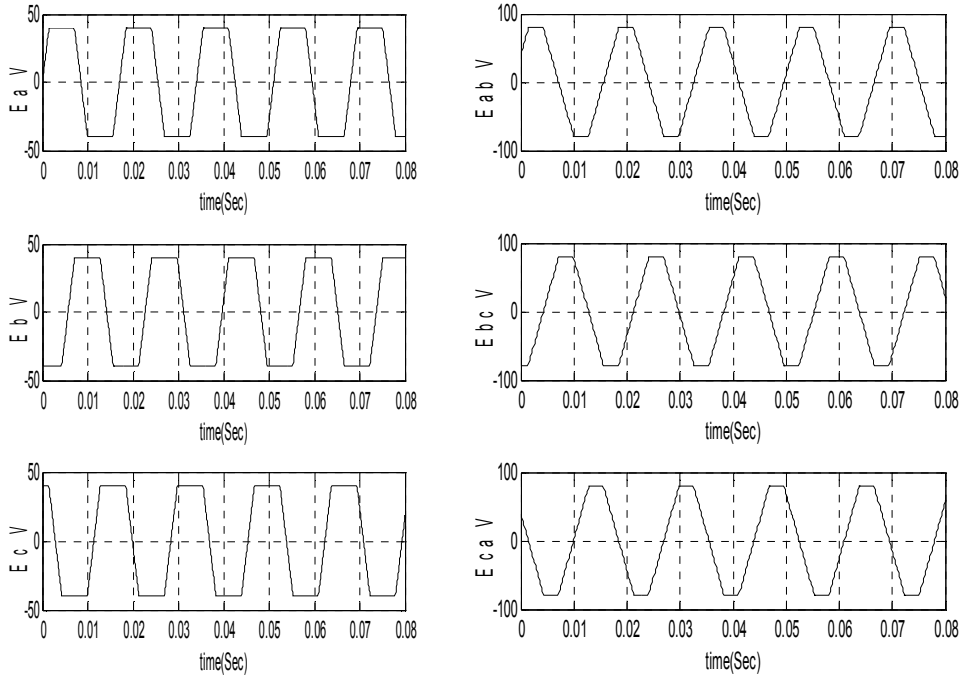

a *b*

Fig. 11. *a*) Back EMFs with reference to rotor position, *b*) Line back EMFs

The dynamic response of the speed and the shaft torque (with $T_L = 0$) are shown in Fig. 13-*a* and Fig. 14-*a* respectively. The actual speed follows the desired speed in less than 0.02s as a result of efficient tuning of the PI controller for both the integral and proportional coefficients. When external load torque of $T_L = 0.1$Nm, for example, is added, the system reaches its steady state in more than 0.02 s, which is the steady state time for no-load system as shown in Fig. 13-*b* and Fig. 14-*b*. The nominal load torque is 0.662 Nm according to motor specifications. As an example of abnormal condition, Fig. 14-*c* shows that the shaft torque is almost zero, when the load torque is raised to T_L=1Nm.

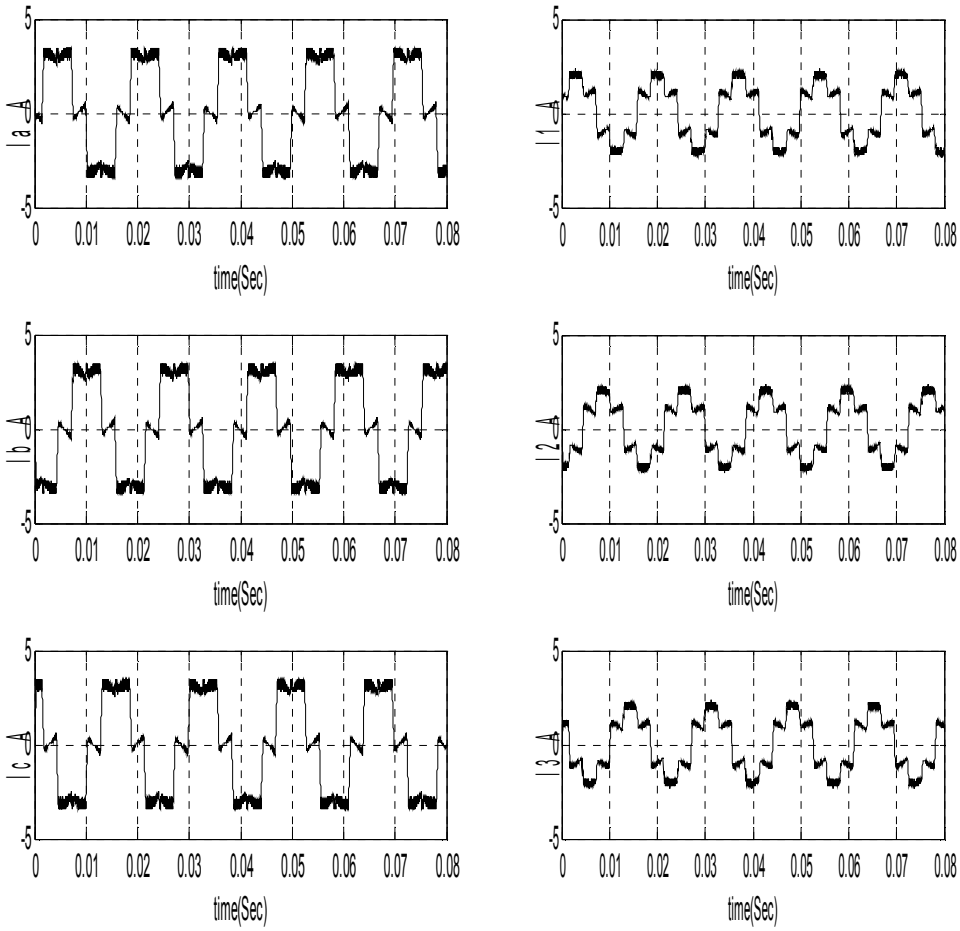

a *b*

Fig. 12. *a*) Phase currents, *b*) Line currents

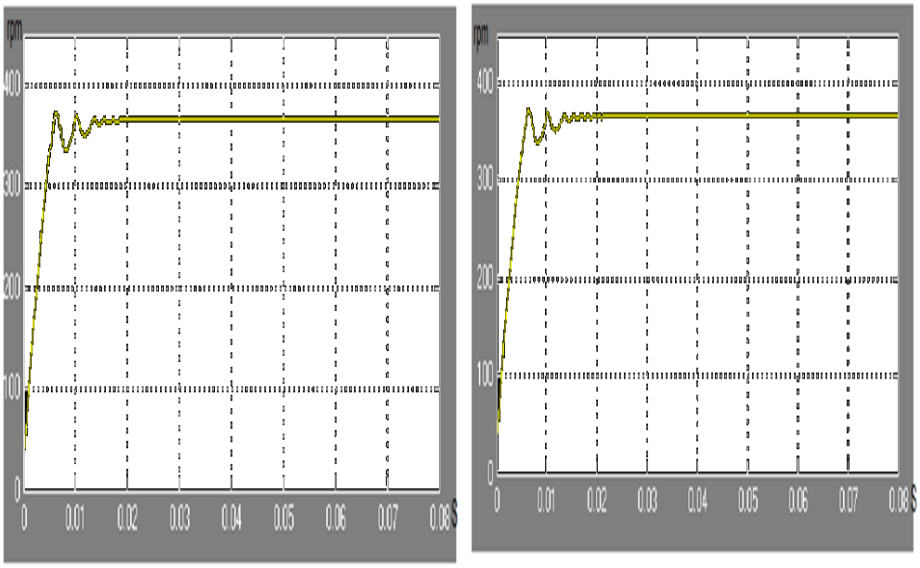

a *b*

Fig. 13. *a*) Speed at no load, *b*) speed with load torque TL=0.1Nm

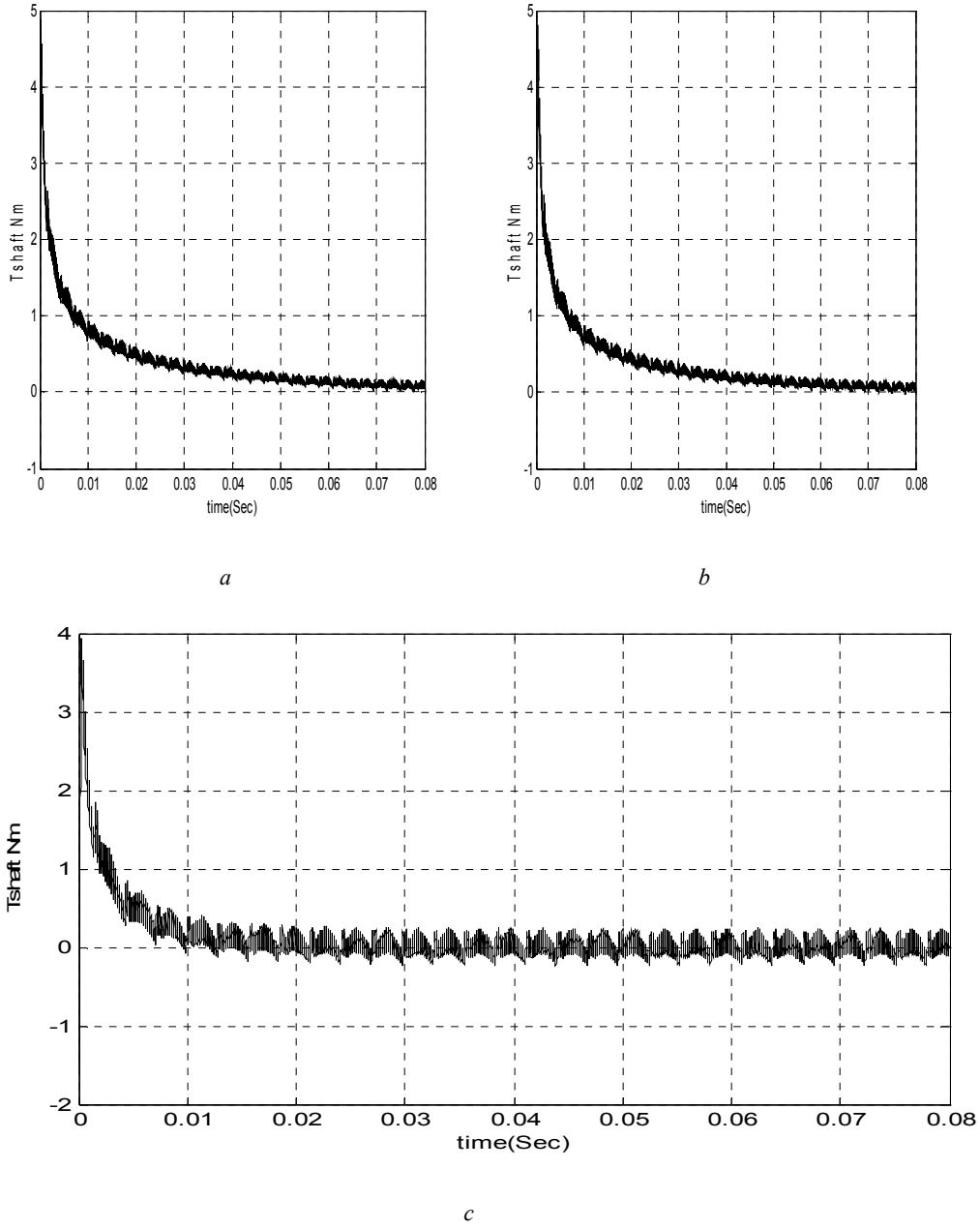

Fig. 14. *a*) Shaft torque at no load, *b*) Shaft torque at T_L=0.1Nm, *c*) Shaft torque at T_L=1Nm (abnormal condition)

The switching functions are shown in Fig. 15-*a*. These functions are generated during the 120˚conduction periods in order to allow the currents to be switched between the upper and lower bands. Fig. 15-*b* shows the expanded version of switching function. The positive value (1) represents the upper band and the negative value (-1) represents the lower band.

The phase voltages and line-to-line voltage are shown in Fig. 16-*a* and 16-*b* respectively. Other values such as the diode, transistor voltages and currents can be obtained easily and analyzed to see their characteristics during switching modes. Also, the external load torque can be varied and monitored to see its effect on the actual speed and to test the efficiency of control blocks in order to quickly reach the desired speed.

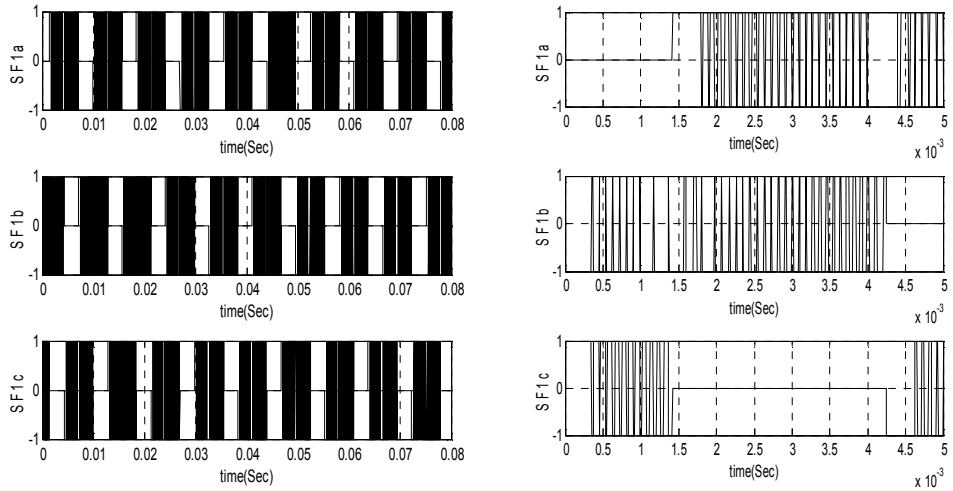

a *b*

Fig. 15. *a*) Switching functions *a*, *b* and *c*, *b*) Expanded switching function

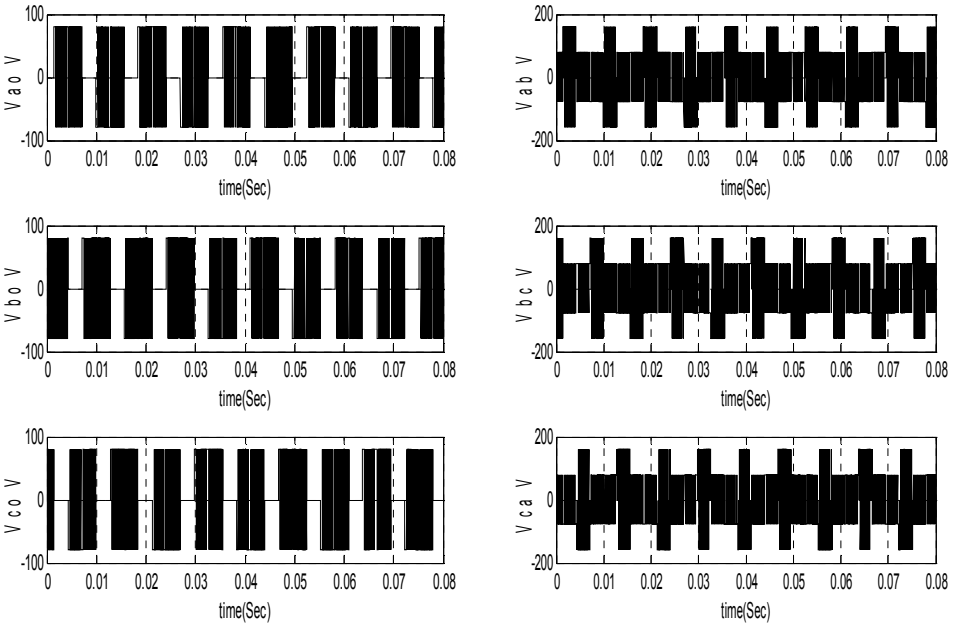

a *b*

Fig. 16. *a*) Phase voltages, *b*) Line voltages

V. CONCLUSION

The analysis of the dynamic as well as the electrical characteristics of the BLDCM has been conducted with the aid of MATLAB environment. The BLDCM model adopted in this work accounts for the effect of friction torque as well as other BLDCM parameters. A reliable model for switching functions has been added. Besides the effect of external load torque, results in time domain for torque, speed, back EMF, phase and line voltages and currents have been monitored and analyzed. Any abnormal conditions can be simulated and analyzed without changing the model. The hardware implementation of this work could be

implemented with recent development of the available DSP kits such as Texas Instruments DRV8301 motor driver which integrates a buck regulator, gate driver, and control logic in a single package.

REFERENCES

[1] J. R. Hendershot and T. J. E. Miller, *Design of Brushless Permanent-Magnet Motor,* Oxford Science, 1994.

[2] J. P. Johnson and M. Ehsani, "Review of sensorless methods for brushless DC," *Proc. of the IEEE Industry Application Society Annual Meeting IAS'99,* pp. 143–150, 1999.

[3] S. K. Safi, P. P. Acarnley, and A. G. Jack, "Analysis and simulation of the high-speed torque performance of brushless DC motor drives," *Proc. of the IEE,* vol. 142, no. 3, pp. 191-200, 1995.

[4] B. K. Lee and M. Ehsani, "A simplified functional model for 3-phase voltage-source inverter using switching function concept," *IEEE Trans. on Industrial Electronics,* vol. 48, no. 2, pp. 309–321, 2001.

[5] B. K. Lee and M. Ehsani, "Advanced simulation model for brushless DC motor drives," *Electric Power Components and Systems,* vol. 31, pp. 841–868, 2003.

[6] M. Cunkaand and O. Aydoğdu, "Releization controller brushless DC motor drives using MATLAB/Simulink," *Mathematical and Computational Applications,* vol. 15, no. 2, pp. 218-229, 2010.

[7] W. Hong, W. Lee, and B. K. Lee, "Dynamic simulation of brushless DC motor drives considering phase commutation for automotive applications," *Proc. of the IEEE Electric Machines & Drives Conference IEMDC'07,* vol. 2, pp. 1377-1383, 2007.

[8] J. Figueroa, C. Brocart, J. Cros, and P. Viarouge, "Simplified simulation methods for polyphase brushless DC motors," *Mathematics and Computers in Simulation,* vol. 63, no. 3-5, pp. 209-224, 2003.

[9] C. W. Hung, C. T. Lin, and C. W. Liu, "An efficient simulation technique for the variable sampling effect of BLDC motor applications," *Proc. of 33rd Annual Conference of IEEE Industrial Electronics IECON 2007,* pp. 1175– 1179, 2007.